Sains Malaysiana 47(9)(2018): 2213–2221
http://dx.doi.org/10.17576/jsm-2018-4709-32

Ingham Problem for Mixed Convection Flow of a Nanofluid over a Moving Vertical Plate with Suction and Injection Effects

(Masalah Ingham untuk Aliran Olakan Campuran bagi Nanobendalir terhadap Plat Telap Menegak yang Bergerak dengan Kesan Sedutan dan Semburan)

ANUAR JAMALUDIN, ROSLINDA NAZAR* & IOAN POP

ABSTRACT

In this study, the effects of suction and injection on the mixed convection flow of a nanofluid, over a moving permeable vertical plate were discussed. A similarity variable was used to transform the governing equations to the ordinary differential equations, which were then solved numerically using the bvp4c programme from MATLAB. Dual solutions (upper and lower branches) were found within a certain range of the mixed convection parameter in assisting and opposing flow regions. A stability analysis was implemented to confirm that the upper branch solution was stable, while the lower branch solution was unstable.

Keywords: Injection; mixed convection; moving plate; nanofluid; stability analysis; suction

ABSTRAK

Dalam kajian ini, kesan sedutan dan semburan pada aliran olakan campuran bagi nanobendalir terhadap plat telap menegak yang bergerak dibincangkan. Pemboleh ubah keserupaan digunakan untuk menjelmakan persamaan menakluk kepada persamaan terbitan biasa dan seterusnya diselesaikan secara berangka menggunakan program bvp4c daripada MATLAB. Penyelesaian dual (cabang atas dan cabang bawah) didapati wujud dalam julat tertentu bagi parameter olakan campuran di dalam kawasan aliran membantu dan aliran menentang. Analisis kestabilan dilakukan bagi mengesahkan bahawa penyelesaian cabang atas adalah stabil, manakala penyelesaian cabang bawah adalah tidak stabil.

Kata kunci: Analisis kestabilan; nanobendalir; olakan campuran; plat bergerak; sedutan; semburan

INTRODUCTION

Mixed convection flow, or combined free and forced convection flow, occurs when both free and forced convection mechanisms coexist and contribute to the heat transfer. Globally, mixed convection flow has become increasingly significant in the heat transfer research, from which various engineering applications have been invented. Some of the remarkable applications are electronic cooling, nuclear reactors technology and nanotechnology. Due to vast range of mixed convection applications in engineering, it has therefore attracted considerable attention of researchers recently (Mamourian et al. 2016; Shirvan et al. 2017a; Zeeshan et al. 2017a). Generally, mixed convection flow can be characterized by two types of flow, the opposing and the assisting flows. Opposing flows refer to the flows for which the buoyancy force has a component opposite to the free stream velocity. On the other hand, the flows for which the buoyancy force has a positive component in the direction of the free stream velocity, are designated as the assisting flows.

Over the past decade, numerous studies of the mixed convection flow have emphasized the existence of dual solutions for the opposing and assisting flows, in a certain range of the buoyancy (or mixed convection) parameter. Ramachandran et al. (1988) studied the laminar mixed convection in stagnation flows adjacent to the vertical surfaces. It was established that the solutions were non-unique in a certain range of the buoyancy parameter, in the opposing flow region. Devi et al. (1991) extended the work of Ramachandran et al. (1988) for the unsteady flow, and the results of the study were in agreement with that obtained by Ramachandran et al. (1988). In contrast to Devi et al. (1991) and Ramachandran et al. (1988), Ishak et al. (2010) and Rhida (1996) reported that dual solutions existed in both the opposing and the assisting flow regions. This finding was supported by Nazar and Pop (2004), Rahman et al. (2015), Roşca et al. (2014) and recently by Abbasbandy et al. (2017), who similarly demonstrated the existence of dual solutions in the mixed convection boundary layer flow.

In the current heat transfer research, the study of nanofluids remained an area of interest due to its various applications, such as medical applicances, coolants for nuclear reactors, solar water heating, cooling of power electronics and directed energy weapons, cooling and heating of buildings and diesel combustion (Saidur et al. 2011; Zeeshan et al. 2017b). Nanofluids are defined as dilute suspension of the solid nanoparticles of diameter 1-100 nm in conventional heat transfer base fluids, for example water, oil, ethylene glycol or glycerol. Nanoparticles are

made from various materials, such as copper (Cu), alumina (Al_2O_3), titania (TiO_2), silver (Ag) and copper oxide (CuO). Two models have been widely used to study the boundary layer flow and the heat transfer of nanofluids, namely Buongiorno model (2006) and Tiwari-Das model (2007). The Buongiorno model highlights the Brownian motion and thermophoresis effects, while the Tiwari-Das model focuses on the volumetric fraction of nanoparticles. More importantly, the boundary layer problem of mixed convection flow in nanofluids have been recently reported by Noor et al. (2015), Subhashini et al. (2014) and recently by Ibrahim et al. (2017), Mabood et al. (2017) and Othman et al. (2017). Despite the completion of many studies, the topic remained a research area for further exploration. In fact, in recent years, there has been increasing interest towards studying the various problems of flow and heat transfer in a nanofluid with different physical conditions (Md. Basir et al. 2017; Ellahi et al. 2017; Hassan et al. 2017; Mohamed et al. 2016; Rashidi et al. 2017; Shirvan et al. 2017b; Zaimi et al. 2017). The studies by Bachok et al. (2016), Mansur et al. (2015), Nazar et al. (2014) and Roşca and Pop (2017) investigated the dual solutions for the problem of boundary layer flow and heat transfer of nanofluids are also worthy of mention.

The objective of this paper was therefore, to study the mixed convection flow near a moving permeable vertical plate, in a nanofluid using the Tiwari-Das model. To be exact, the present paper is an extension of the classical work of Ingham (1986) from the free convection boundary layer flow to the mixed convection boundary layer flow. In this study, the boundary layer equations describing the problem are reduced into ordinary differential equations using similarity variables. The equations are then solved numerically using the bvp4c programme from MATLAB. The novel results presented in this study demonstrated that there are dual (upper and lower branch) solutions, in a certain range of the suction/injection parameter and the mixed convection parameter. In addition, stability analysis of the dual solutions, is performed to prove the stability and instability of the upper and lower branch solutions, respectively. The results of this paper are original and different from the previous studies (Bachok et al. 2011; Ingham 1986), having provided important insights on the industrial applications of mixed convection flow of a nanofluid.

BASIC EQUATIONS

This study considers a two-dimensional mixed convection flow of a viscous and incompressible fluid, over a permeable vertical flat plate. The flat plate which originates from a slot, is assumed to be moving with a constant speed U_0 in a vertical direction. In the present study, the fluid refers to water-based nanofluid that contains different types of nanoparticles, such as copper (Cu), alumina (Al_2O_3) and titania (TiO_2). The thermophysical properties of these base fluid and nanoparticles are given in Table 1 (Oztop & Abu-Nada 2008). The coordinate system has its origin located at the slot, with the positive $\bar{x}$ extending along the plate and in the direction of motion, while the $\bar{y}$ axis is measured normal to the plate in the positive direction from the plate to the fluid.

TABLE 1. Thermophysical properties of the base fluid and the nanoparticles

Physical properties	Water	Cu	Al_2O_3	TiO_2
$C_p\,(J\,kg^{-1}K^{-1})$	4179	385	765	686.2
$\rho\,(kg\,m^{-3})$	997.1	8933	3970	4250
$k\,(W\,m^{-1}\,K^{-1})$	0.613	400	40	8.9538
$\beta \times 10^{-5}\,(K^{-1})$	21	1.67	0.85	0.9

In the formulation of the problem, the surface of the plate is maintained at a temperature $T_w = T_\infty + T_1/(\bar{x}/l)$, where T_∞ is the ambient fluid temperature; T_1 is a reference temperature; and l is a reference length. Additionally, the cooling and heating of the moving plate are taken into consideration. Furthermore, the fluid properties are assumed to be constant, except that the density variations within the fluid are allowed to induce buoyancy forces, which corresponds to the Boussinesq approximation. Under such conditions and following the nanofluid model proposed by Tiwari and Das (2007), the governing boundary layer equations in dimensional form are (Ingham 1986):

$$\frac{\partial \bar{u}}{\partial \bar{x}} + \frac{\partial \bar{v}}{\partial \bar{y}} = 0 \tag{1}$$

$$\bar{u}\frac{\partial \bar{u}}{\partial \bar{x}} + \bar{v}\frac{\partial \bar{u}}{\partial \bar{y}} = \frac{\mu_{nf}}{\rho_{nf}}\frac{\partial^2 \bar{u}}{\partial \bar{y}^2} + \frac{(\rho\beta)_{nf}}{\rho_{nf}}\left(\bar{T} - T_\infty\right)g \tag{2}$$

$$\bar{u}\frac{\partial \bar{T}}{\partial \bar{x}} + \bar{v}\frac{\partial \bar{T}}{\partial \bar{y}} = \alpha_{nf}\frac{\partial^2 \bar{T}}{\partial \bar{y}^2} \tag{3}$$

along with the boundary conditions

$$\bar{u} = U_0, \bar{v} = \bar{v}_w(\bar{x}), \bar{T} = T_w \text{ at } \bar{y} = 0$$

$$\bar{u} \to 0, \bar{T} \to T_\infty \text{ as } \bar{y} \to \infty \tag{4}$$

where $\bar{u}$ and $\bar{v}$ represent the velocity components in the $\bar{x}$ and $\bar{y}$ directions, respectively, and g is the acceleration due to gravity. In addition, μ_{nf} is the dynamic viscosity of the nanofluid, which was described by the Brinkman model, ρ_{nf} is the density of the nanofluid, $(\rho\beta)_{nf}$ is the thermal expansion coefficient of the nanofluid and α_{nf} is the thermal diffusivity of the nanofluid, which are given by (Oztop & Abu-Nada 2008).

$$\mu_{nf}=\frac{\mu_f}{(1-\phi)^{2.5}},\ \alpha_{nf}=\frac{k_{nf}}{\left(\rho C_p\right)_{nf}}$$
$$\rho_{nf}=\left(1-\phi\right)\rho_f+\phi\rho_s$$
$$\left(\rho\beta\right)_{nf}=\left(1-\phi\right)\left(\rho\beta\right)_f+\phi\left(\rho\beta\right)_s \quad (5)$$
$$\left(\rho C_p\right)_{nf}=\left(1-\phi\right)\left(\rho C_p\right)_f+\phi\left(\rho C_p\right)_s$$
$$\frac{k_{nf}}{k_f}=\frac{k_s+2k_f-2\phi\left(k_f-k_s\right)}{k_s+2k_f+\phi\left(k_f-k_s\right)}$$

where μ_f is the dynamic viscosity of the base fluid; ϕ is the nanoparticle volume fraction; ρ_f and ρ_s are the densities of the base fluid and the solid nanoparticle, respectively, $(\rho C_p)_{nf}$ is the heat capacitance of the nanofluid; k_{nf} is the thermal conductivity of the nanofluid, as approximated by Maxwell-Garnett model and k_f and k_s are the thermal conductivities of the base fluid and the solid nanoparticle, respectively. Furthermore, the following non-dimensional boundary layer variables are defined as (Ingham 1986):

$$x=\overline{x}/l,\quad y=\mathrm{Re}^{1/2}\,\overline{y}/l,\quad u=\overline{u}/U_0,\quad v=\mathrm{Re}^{1/2}\,\overline{v}/U_0$$
$$v_w=\mathrm{Re}^{1/2}\,\overline{v}_w/U_0,\quad T=\left(\overline{T}-T_\infty\right)/T_1 \quad (6)$$

where Re is the Reynolds number ($=U_0 l/\nu_f$). Substituting (6) into (1)-(3), the following non-dimensional boundary layer equations are obtained:

$$\frac{\partial u}{\partial x}+\frac{\partial v}{\partial y}=0 \quad (7)$$

$$u\frac{\partial u}{\partial x}+v\frac{\partial u}{\partial y}=\frac{\rho_f}{\rho_{nf}}\left(\frac{1}{\left(1-\phi\right)^{2.5}}\frac{\partial^2 u}{\partial y^2}+\left(1-\phi+\phi\frac{\left(\rho\beta\right)_s}{\left(\rho\beta\right)_f}\right)\frac{\lambda}{2}T\right) \quad (8)$$

$$u\frac{\partial T}{\partial x}+v\frac{\partial T}{\partial y}=\frac{1}{\mathrm{Pr}}\frac{\alpha_{nf}}{\alpha_f}\frac{\partial^2 T}{\partial y^2} \quad (9)$$

Here $\lambda = 2\,g\beta_f T_1 l/U_0^2 = 2Gr/\mathrm{Re}^2$ is the mixed convection parameter, with $\lambda > 0$ corresponding to the assisting flow, and $\lambda < 0$ corresponding to the opposing flow, $Gr = g\beta_f T_1 l^3/\nu_f^2$ is the Grashof number and $\mathrm{Pr} = \nu_f/\alpha_f$ is the Prandtl number. In addition, the boundary conditions (4) become,

$$u=1,\ v=v_w(x),\ T=1/x \ \text{ at } \ y=0$$
$$u\to 0, T\to 0 \ \text{ as } \ y\to\infty \quad (10)$$

where $v_w(x)$ is the mass flux velocity with $v_w<0$ for suction and $v_w>0$ for blowing or injection. In the order that the similarity solutions of (7)-(9) along with the boundary conditions (10) exist, $v_w(x)$ is assumed to be the following form (Bachok et al. 2011):

$$v_w\left(x\right)=-\frac{1}{\sqrt{2x}}f\left(0\right) \quad (11)$$

Moreover, to obtain the similarity solutions of the (7)-(9) subject to the boundary conditions (10), the following similarity variables are introduced (Ingham 1986):

$$\eta=\frac{1}{\sqrt{2x}}y,\quad \psi=\sqrt{2x}f\left(\eta\right),\quad T=\frac{1}{x}\theta\left(\eta\right) \quad (12)$$

where ψ is the non-dimensional stream function defined in the usual way as,

$$u=\frac{\partial\psi}{\partial y},\quad v=-\frac{\partial\psi}{\partial x} \quad (13)$$

which identically satisfy the continuity (7). Employing the similarity variables (12) into the (7)-(9), (8) and (9) are reduced to the following ordinary differential equations:

$$\frac{1}{\left(1-\phi\right)^{2.5}}f'''+\left(1-\phi+\phi\frac{\rho_s}{\rho_f}\right)ff''+\left(1-\phi+\phi\frac{\left(\rho\beta\right)_s}{\left(\rho\beta\right)_f}\right)\lambda\theta=0 \quad (14)$$

$$\frac{1}{\mathrm{Pr}}\frac{k_{nf}}{k_f}\theta''+\left(1-\phi+\phi\frac{\left(\rho C_p\right)_s}{\left(\rho C_p\right)_f}\right)\left(f\theta'+2f'\theta\right)=0 \quad (15)$$

and the boundary conditions (10) become

$$f(0)=s,\ f'(0)=1,\ \theta(0)=1$$
$$f'(\eta)\to 0,\ \theta(\eta)\to 0 \ \text{ as } \ \eta\to\infty \quad (16)$$

where primes denote differentiation with respect to η; s is a constant which determines the transpiration rate; with $s>0$ for suction; $s<0$ for injection and $s=0$ for an impermeable surface. It is worth highlighting that when $\phi=0$ and $s=0$, (14) and (15) with the boundary conditions (16) are reduced to those found by Ingham (1986).

STABILITY OF SOLUTIONS

In the present research, the numerical results of (14) and (15) subject to the boundary conditions (16) show that there are two branches of solutions for different values of the suction/injection parameter s. Therefore, the stability of the dual (upper and lower branch) solutions is evaluated. The stability of the dual solutions is determined by adapting the stability analysis (Merkin 1985; Weidman et al. 2006). To perform a stability analysis, the unsteady form of the problem derived in previous section is considered. Equation (7) is held, while (8) and (9) are replaced by,

$$\frac{\partial u}{\partial t}+u\frac{\partial u}{\partial x}+v\frac{\partial u}{\partial y}=\frac{\rho_f}{\rho_{nf}}\left(\frac{1}{\left(1-\phi\right)^{2.5}}\frac{\partial^2 u}{\partial y^2}+\left(1-\phi+\phi\frac{\left(\rho\beta\right)_s}{\left(\rho\beta\right)_f}\right)\frac{\lambda}{2}T\right) \quad (17)$$

$$\frac{\partial T}{\partial t}+u\frac{\partial T}{\partial x}+v\frac{\partial T}{\partial y}=\frac{1}{\mathrm{Pr}}\frac{\alpha_{nf}}{\alpha_f}\frac{\partial^2 T}{\partial y^2} \tag{18}$$

where t denotes the time. Based on the similarity variables (12), the new similarity variables for the unsteady (17) and (18) are,

$$\eta=\frac{1}{\sqrt{2x}}y,\quad \tau=\frac{1}{2x}t,\quad \psi=\sqrt{2x}f\left(\eta,\tau\right),\quad T=\frac{1}{x}\theta\left(\eta,\tau\right) \tag{19}$$

Substituting the similarity variables (19) into (17) and (18), the following equations are derived:

$$\frac{1}{\left(1-\phi\right)^{2.5}}\frac{\partial^3 f}{\partial\eta^3}+\left(1-\phi+\phi\frac{\rho_s}{\rho_f}\right)$$
$$\left(f\frac{\partial^2 f}{\partial\eta^2}+2\tau\left(\frac{\partial f}{\partial\eta}\frac{\partial^2 f}{\partial\eta\partial\tau}-\frac{\partial f}{\partial\tau}\frac{\partial^2 f}{\partial\eta^2}\right)-\frac{\partial^2 f}{\partial\eta\partial\tau}\right)$$
$$+\left(1-\phi+\phi\frac{\left(\rho\beta\right)_s}{\left(\rho\beta\right)_f}\right)\lambda\theta=0 \tag{20}$$

$$\frac{1}{\mathrm{Pr}}\frac{k_{nf}}{k_f}\frac{\partial^2\theta}{\partial\eta^2}+\left(1-\phi+\phi\frac{\left(\rho C_p\right)_s}{\left(\rho C_p\right)_f}\right)$$
$$\left(f\frac{\partial\theta}{\partial\eta}+2\frac{\partial f}{\partial\eta}\theta+2\tau\left(\frac{\partial f}{\partial\eta}\frac{\partial\theta}{\partial\tau}-\frac{\partial f}{\partial\tau}\frac{\partial\theta}{\partial\eta}\right)-\frac{\partial\theta}{\partial\tau}\right)=0 \tag{21}$$

subject to the boundary conditions

$$f\left(0,\tau\right)=s,\ \frac{\partial f}{\partial\eta}\left(0,\tau\right)=1,\ \theta\left(0,\tau\right)=1$$
$$\frac{\partial f}{\partial\eta}\left(\eta,\tau\right)=0,\ \theta\left(\eta,\tau\right)=0\ \text{as}\ \eta\to\infty \tag{22}$$

To determine the stability of the solution $f(\eta)=f_0(\eta)$ and $\theta(\eta)=\theta_0(\eta)$ satisfying the equations (14) and (15) with the boundary conditions (16), we follow Weidman et al. (2006) and Rosca et al. (2014) and write

$$f\left(\eta,\tau\right)=f_0\left(\eta\right)+e^{-\gamma\tau}F\left(\eta,\tau\right),\quad \theta\left(\eta,\tau\right)=\theta_0\left(\eta\right)+e^{-\gamma\tau}G\left(\eta,\tau\right) \tag{23}$$

where γ is an unknown eigenvalues. Furthermore, $F(\eta,\tau)$ and $G(\eta,\tau)$ are assumed to be small relative to $f_0(\eta)$ and $\theta(\eta)$. Substituting (23) into (20) and (21), the following equations are generated:

$$\frac{1}{\left(1-\phi\right)^{2.5}}\frac{\partial^3 F}{\partial\eta^3}+\left(1-\phi+\phi\frac{\rho_s}{\rho_f}\right)\left[f_0\frac{\partial^2 F}{\partial\eta^2}+f_0''F+2\tau\right.$$
$$\left.\left(-\gamma f_0'\frac{\partial F}{\partial\eta}+f_0'\frac{\partial^2 F}{\partial\eta\partial\tau}+\gamma f_0''F-f_0''\frac{\partial F}{\partial\tau}\right)\right.$$
$$\left.+\gamma\frac{\partial F}{\partial\eta}-\frac{\partial^2 F}{\partial\eta\partial\tau}\right]+\left(1-\phi+\phi\frac{\left(\rho\beta\right)_s}{\left(\rho\beta\right)_f}\right)\lambda G=0 \tag{24}$$

$$\frac{1}{\mathrm{Pr}}\frac{k_{nf}}{k_f}\frac{\partial^2 G}{\partial\eta^2}+\left(1-\phi+\phi\frac{\left(\rho C_p\right)_s}{\left(\rho C_p\right)_f}\right)$$
$$\left[f_0\frac{\partial G}{\partial\eta}+\theta_0'F+2\left(f_0'G+\theta_0\frac{\partial F}{\partial\eta}\right)\right.$$
$$\left.+2\tau\left(-\gamma f_0'G+f_0'\frac{\partial G}{\partial\tau}+\gamma\theta_0'F-\theta_0'\frac{\partial F}{\partial\tau}\right)+\gamma G-\frac{\partial G}{\partial\tau}\right]=0 \tag{25}$$

along with the boundary conditions,

$$F\left(0,\tau\right)=0,\ \frac{\partial F}{\partial\eta}\left(0,\tau\right)=0,\ G\left(0,\tau\right)=0$$
$$\frac{\partial F}{\partial\eta}\left(\eta,\tau\right)=0,\ G\left(\eta,\tau\right)=0\ \text{as}\ \eta\to\infty \tag{26}$$

As suggested by Weidman et al. (2006), the stability of solution $f_0(\eta)$ and $\theta_0(\eta)$ of (14) and (15), subject to the boundary conditions (16), is determined by setting $\tau=0$. From which, $F=F_0(\eta)$ and $G=G_0(\eta)$ are obtained in (24) and (25) to identify the initial growth or decay of the solution (23). To evaluate the numerical procedure, the following linear eigenvalue equations are tested:

$$\frac{1}{\left(1-\phi\right)^{2.5}}F_0'''+\left(1-\phi+\phi\frac{\rho_s}{\rho_f}\right)\left(f_0F_0''+f_0''F_0+\gamma F_0'\right)$$
$$+\left(1-\phi+\phi\frac{\left(\rho\beta\right)_s}{\left(\rho\beta\right)_f}\right)\lambda G_0=0 \tag{27}$$

$$\frac{1}{\mathrm{Pr}}\frac{k_{nf}}{k_f}G_0''+\left(1-\phi+\phi\frac{\left(\rho C_p\right)_s}{\left(\rho C_p\right)_f}\right)$$
$$\left(f_0G_0'+F_0\theta_0'+2\left(f_0'G_0+\theta_0F_0'\right)+\gamma G_0\right)=0 \tag{28}$$

together with the boundary conditions

$$F_0\left(0\right)=0,\ F_0'\left(0\right)=0,\ G_0\left(0\right)=0$$
$$F_0'\left(\eta\right)=0,\ G_0\left(\eta\right)=0\ \text{as}\ \eta\to\infty \tag{29}$$

According to Harris et al. (2009), the range of possible eigenvalues could be investigated by relaxing an appropriate boundary condition on $F_0'(\eta)$ or $G_0(\eta)$. In the case of the present problem, the boundary condition $F_0'(\eta)\to 0$ is relaxed as $\eta\to\infty$ and an additional boundary condition, $F_0''(0)=1$ is enforced.

The solutions $f_0(\eta)$ and $\theta_0(\eta)$ are determined from (14) and (15) along with the boundary conditions (16), before being substituted into (27) and (28), in which the linear eigenvalue problem (27)-(29) could be solved.

Furthermore, the solution of the linear eigenvalue problem (27)-(29) gives an infinite set of possible eigenvalues $\gamma_1 < \gamma_2 < \gamma_3 < \ldots$, where γ_1 is the smallest eigenvalue. It is also established that for particular values of λ, s and other parameters involved, the stability of the solutions $f_0(\eta)$ and $\theta_0(\eta)$ is determined by the smallest eigenvalue γ_1. A positive smallest eigenvalue γ_1 indicates an initial decay of disturbances and a stable solution. On the contrary, a negative smallest eigenvalue γ_1 represents an initial growth of disturbances and an unstable solution.

Results and Discussion

Equations (14) and (15) subject to the boundary conditions (16) are solved numerically for selected values of the suction/injection parameter s and the mixed convection parameter λ. Meanwhile, the nanoparticle volume fraction ϕ and the Prandtl number are fixed to 0.01 and 6.2 (water), respectively, except for comparison with the previously reported cases. These equations are solved numerically using the bvp4c programme which is considered an effective solver from MATLAB (Shampine et al. 2000). The relative error tolerance is set at 10^{-3}. In addition, a suitable finite value of $\eta \to \infty$, namely $\eta = \eta_\infty = 10$, is selected. The values of reduced skin friction coefficient $f''(0)$, and reduced heat transfer rate $-\theta'(0)$ for $s = 0$ (impermeable plate), $\phi = 0$, Pr = 1 and for some values of $\lambda > 0$ (assisting flow), are obtained and compared with the previous studies. These comparisons, shown in Tables 2 and 3, showed the consistency of the present results with that reported by Bachok et al. (2011) and Ingham (1986). Hence, the findings from this study are established as correct and accurate.

On further examination of the results, the existence of dual (upper and lower branch) solutions is demonstrated by some values of λ and s. As mentioned earlier, stability analysis is performed in this study to evaluate the stability of the dual solutions. A search for the smallest eigenvalues γ_1 satisfying (27)-(29) is conducted using the bvp4c programme from MATLAB, and the results are given in Table 4. The results clearly show that the upper and lower branch solutions are represented by $\gamma_1 > 0$ and $\gamma_1 < 0$, respectively. These results are consistent with the findings reported by other studies (Bachok et al. 2016; Mansur 2015; Nazar 2014; Roşca & Pop 2017). The upper branch solution is therefore stable, whereas the lower branch solution is unstable.

TABLE 2. Comparison of $f''(0)$ for several values of λ on the upper branch solution

λ	Ingham (1986)	Bachok et al. (2011)	Present
1	24.89	24.8852	24.885306
0.8	25.85	25.8492	25.849276
0.6	26.77	26.7693	26.769332
0.4	27.76	27.6520	27.652049
0.2	28.50	28.5025	28.502463
0.1	28.92	28.9169	28.916882
0.05	29.12	29.1216	29.121604
0.02	29.28	29.2436	29.243645
0.01	29.31	29.2842	29.284198

TABLE 3. Comparison of $-\theta'(0)$ for several values of λ on the upper branch solution

λ	Ingham (1986)	Bachok et al. (2011)	Present
1	300.5	300.5307	300.531798
0.8	399.9	399.8621	399.863430
0.6	564.7	564.7015	564.703197
0.4	893.5	893.4901	893.492585
0.2	1878.4	1878.3499	1878.351645
0.1	3847.1	3847.0781	3847.083856
0.05	7784.1	7784.0798	7784.100435
0.02	19594.0	19594.7367	19594.788056
0.01	39279.0	39279.0511	39279.153569

TABLE 4. Smallest eigenvalues γ_1 for several values of s and λ

s	λ	γ_1(upper branch)	γ_1(lower branch)
–0.1	–1	5.1219	–0.4726
	–3	4.7562	–0.4627
0	–1	4.8256	–0.3633
	–3	4.5946	–0.3958
0.1	–1	4.8177	–0.0063
	–3	4.8729	–0.3367

Figures 1–3 provide the variations of the reduced skin friction coefficients $f''(0)$ and the reduced heat transfer rate $-\theta'(0)$ with λ for $s = -0.1$, $s = 0$ and $s = 0.1$ when $\phi = 0.01$ and Pr = 6.2, for three different types of water-based nanofluids (Cu-water, Al_2O_3-water and TiO_2-water nanofluids). These figures show that it is possible to obtain dual solutions for the assisting flow ($\lambda > 0$), other than that usually reported in the literature for the opposing flow ($\lambda < 0$). In this paper, solid lines refer to the upper branch solution, while the dotted lines represent the lower branch solution. It is evident that the dual solutions exist for (14) and (15), which are subjected to the boundary conditions (16) in the range $\lambda < \lambda c$, where λc is the critical value of λ; a unique solution exists at $\lambda = \lambda c$ and no solution exists when $\lambda > \lambda c$. Moreover, on inspection of these figures showed that the values of the reduced skin friction coefficient and the reduced heat transfer rate are highest for Cu-water nanofluid, followed by TiO_2- and Al_2O_3-water nanofluids. Physically, this is because Cu has the highest value of thermal conductivity compared to the other nanoparticles.

In the case of $\lambda < \lambda c$, the results shown in Figures 1(b), 2(b) and 3(b) for the reduced heat transfer rate $-\theta'(0)$, suggest that for the upper branch solution, $-\theta'(0)$ becomes unbounded as $\lambda \to 0$. The small gap, or better known as the limiting solutions, in the upper branch

solution of around $\lambda = 0$ (Figures 1(a), 2(a) and 3(a)) is due to the lack of a converged numerical solution, since the corresponding behavior of $-\theta'(0)$ (Figures 1(b), 2(b) and 3(b)) is a tendency towards large positive values ($\lambda \to 0^+$) and large negative values ($\lambda \to 0^-$). In relation to the case when $\lambda = \lambda c$, both solution branches are connected, thus a unique solution is obtained. Nevertheless, when $\lambda > \lambda c$, the full Navier-Stokes and energy equations have to be solved, which is beyond the scope of the present paper. Moreover, it is apparent that all the values of λc for Cu-water nanofluid are higher, compared to those of Al_2O_3-water and TiO_2-water nanofluids. It is therefore assumed that the presence of Cu nanoparticles in a water-based nanofluid, is more capable of delaying the boundary layer separation, compared to the Al_2O_3 and TiO_2 nanoparticles.

Additionally, for each value of λ within the range $\lambda < \lambda c$, the values of $f''(0)$ for the upper branch solution raise with the increase of s. This is due to the physical fact that the suction effect at the boundary slows down the fluid motion and thus, increases the velocity gradient at the surface. Similarly, at any λ station within the domain $\lambda < 0$, there is a rise in the values of $-\theta'(0)$ for the upper branch solution with the increase of s. On the contrary, at any λ station within the range $0 < \lambda < \lambda c$, the values of $-\theta'(0)$ for the upper branch solution decrease with the increase of s. Physically, this finding indicates that the greater the magnitude of suction/injection parameter, the higher the heat transfer rate at the surface of the plate in the opposing flow region.

As shown in Figures 1–3, Cu-water nanofluid produces higher values for both the $f''(0)$ and $-\theta'(0)$, compared to those of Al_2O_3-water and TiO_2-water nanofluids. It is observed that the values of $f''(0)$ and $-\theta'(0)$ for Al_2O_3-water and TiO_2-water nanofluids are almost identical. The values of λc are also noted to be higher with the increase of s. This finding suggested that the increase of s widens the range of existence of the solutions for the (14) and (15) with the boundary conditions (16). Hence, the increment of suction/injection parameter could decelerate the separation of the boundary layer in the assisting flow region.

Finally, Figures 4 and 5 provide the samples of the velocity profiles $f'(\eta)$ and the temperature profiles $\theta(\eta)$ for the Cu-water nanofluid, in the opposing flow region with different values of the suction/injection parameter s, when $\lambda = -0.5$, $\phi = 0.01$ and Pr = 6.2. Based on these figures, it is evident that the upper branch solution for the velocity and temperature profiles, displays a thinner boundary layer thickness, compared to the lower branch solution. For example, for $s = 0.1$, upper branch solution of velocity profile displays $\eta_\infty \approx 7$ (Figure 4(a)), while lower branch solution of velocity profile displays $\eta_\infty \approx 10$ (Figure 4(b)). Furthermore, in Figure 4(a), the velocity profiles are shown to rise with the increase of s, whereas the graph presented in Figure 5(a) illustrates a vast reduction in the temperature profiles as s increases. Moreover, the increase of s reduces the thickness of velocity and thermal boundary layers. It is also apparent from Figures 4 and 5 that the profiles for both the upper and lower branch solutions satisfy the far field boundary conditions (16) asymptotically. Therefore, the profiles are significant in validating the numerical results obtained for the equations (14) and (15) subject to the boundary conditions (16). This finding establishes the existence of dual nature of the solutions shown in Figures 1–3 and thus, cannot be neglected mathematically.

Conclusion

In this paper, the well-known classical work of Ingham (1986) on free convection boundary layer flow over a moving vertical impermeable plate, has been extended to the case of mixed convection flow in a nanofluid.

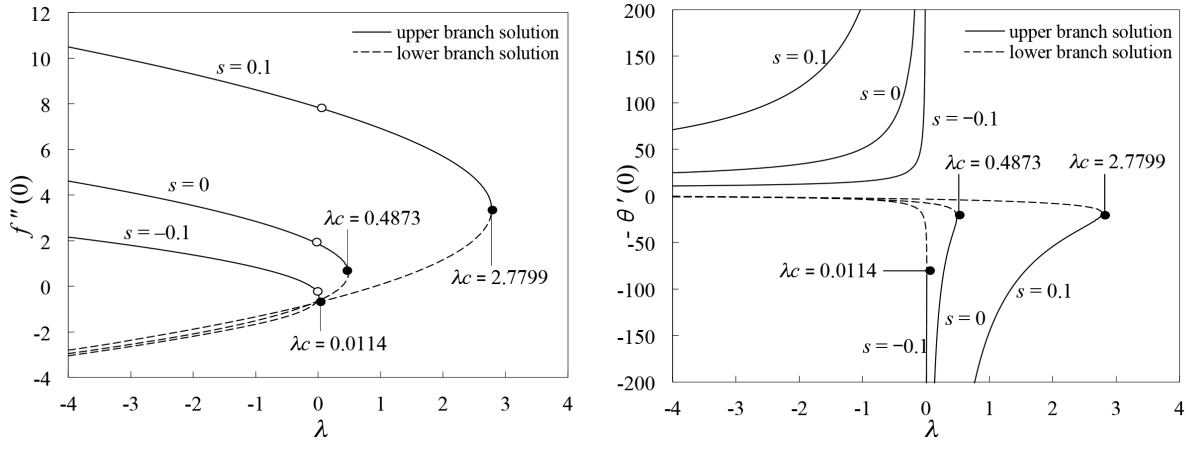

(a) (b)

FIGURE 1. (a) Variation of the reduced skin friction coefficient $f''(0)$ with λ for several values of s for Cu-water nanofluid; (b) Variation of the reduced heat transfer rate $-\theta'(0)$ with λ for several values of s for Cu-water nanofluid

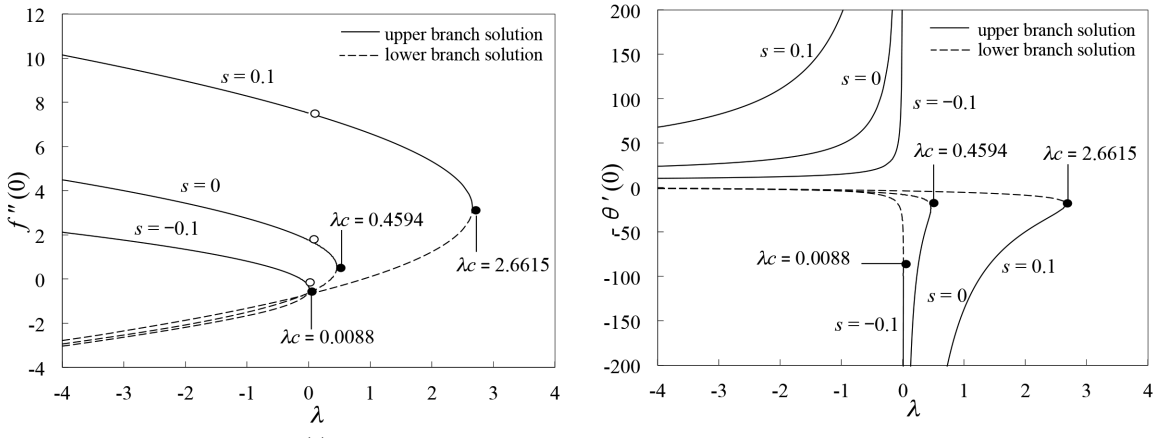

(a) (b)

FIGURE 2. (a) Variation of the reduced skin friction coefficient $f''(0)$ with λ for several values of s for Al_2O_3-water nanofluid; (b) Variation of the reduced heat transfer rate $-\theta'(0)$ with λ for several values of s for Al_2O_3-water nanofluid

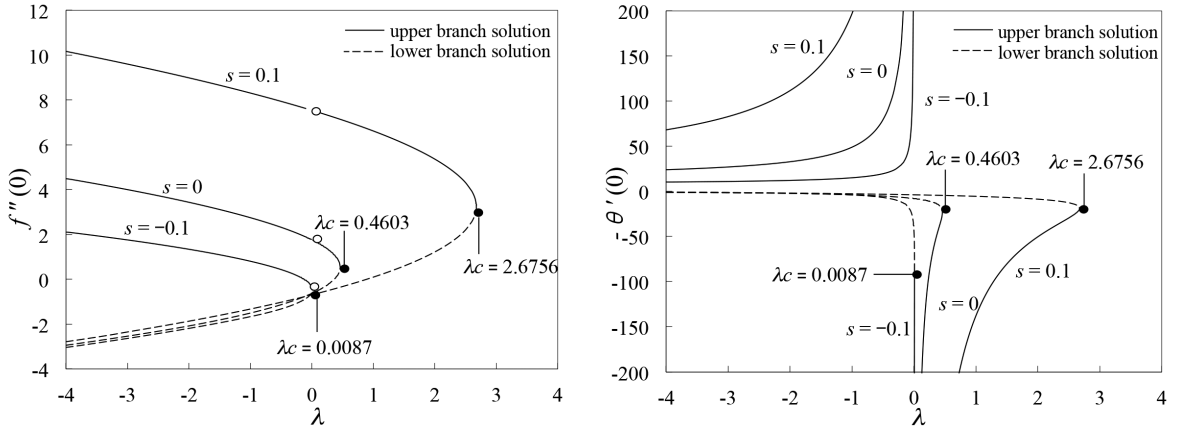

(a) (b)

FIGURE 3. (a) Variation of the reduced skin friction coefficient $f''(0)$ with λ for several values of s for TiO_2-water nanofluid; (b) Variation of the reduced heat transfer rate $-\theta'(0)$ with λ for several values of s for TiO_2-water nanofluid

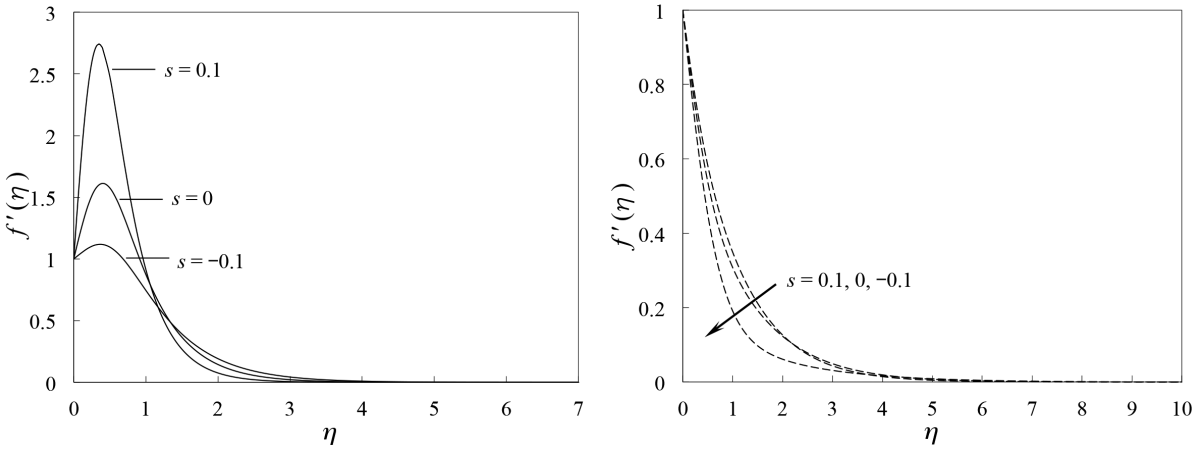

(a) (b)

FIGURE 4. Velocity profiles $f'(\eta)$ for several values of s for Cu-water nanofluid: (a) Upper branch solution; (b) Lower branch solution

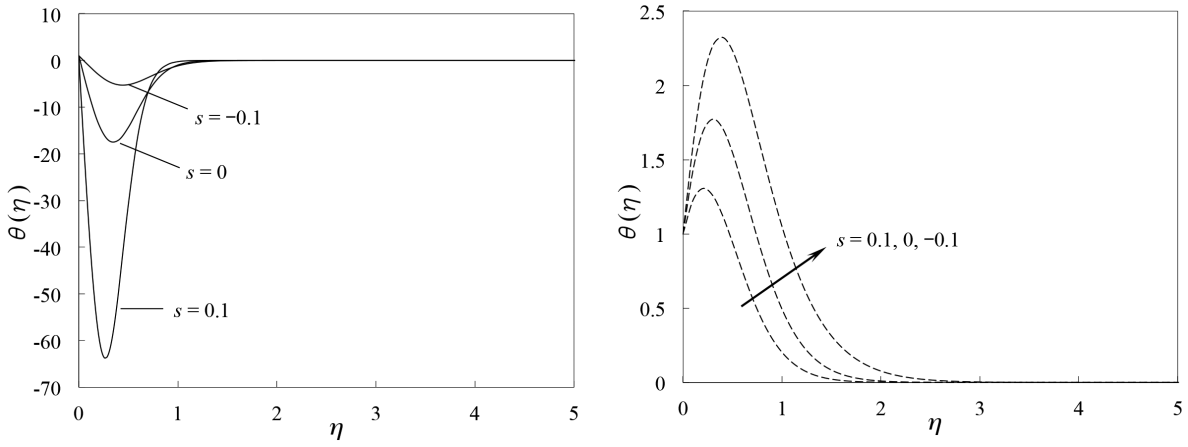

FIGURE 5. Temperature profiles $\theta(\eta)$ for several values of s for Cu-water nanofluid: (a) Upper branch solution and (b) Lower branch solution

Additionally, the effects of suction and injection on Cu-water, Al_2O_3-water and TiO_2-water nanofluids, were imposed by using the nanofluid model proposed by Tiwari and Das (2007). The boundary layer equations describing the problem were reduced into ordinary differential equations using similarity variables. Then, the resulting equations with the associated boundary conditions were solved numerically via the bvp4c programme from MATLAB, in both the assisting and opposing flow cases for selected values of the suction/injection parameter s. Some significant observations of this study were recapitulated as follows:

Dual (upper and lower branch) solutions were obtained for both the assisting and opposing flow. In the opposing flow case, a solution was obtained for all negative values of the mixed convection parameter λ. On the contrary, the solution only existed for a certain range of λ in the assisting flow case. The two branches solutions merged with one another at a critical value, λc, hence, no solution existed when $\lambda > \lambda c$. A stability analysis was conducted to confirm that the upper branch solution was stable, while the lower branch solution was unstable. The value of λc increased with the increase of s. Thus, the boundary layer separation could be delayed by increasing the values of s. Furthermore, Cu-water nanofluid was more capable of delaying the boundary layer separation, compared to the Al_2O_3-water and TiO_2-water nanofluids.

ACKNOWLEDGEMENTS

The present work was supported by the research university grant from Universiti Kebangsaan Malaysia (DIP-2017-009).

REFERENCES

Abbasbandy, S., Shivanian, E., Vajravelu, K. & Kumar, S. 2017. A new approximate analytical technique for dual solutions of nonlinear differential equations arising in mixed convection heat transfer in a porous medium. *Int. J. Numer. Methods Heat Fluid Flow* 27(2): 486-503.

Bachok, N., Najib, N., Arifin, N.M. & Senu, N. 2016. Stability of dual solutions in boundary layer flow and heat transfer on a moving plate in a copper-water nanofluid with slip effect. *WSEAS Transactions on Fluid Mechanics* 11: 151-158.

Bachok, N., Ishak, A., Nazar, R. & Pop, I. 2011. Ingham problem for free convection near a continuously moving vertical permeable plate. *IMA J. Appl. Math.* 77(4): 578-589.

Md. Basir, M.F., Uddin, M.J. & Ismail, A. 2017. Unsteady magnetoconvective flow of bionanofluid with zero mass flux boundary condition. *Sains Malaysiana* 46(2): 327-333.

Buongiorno, J. 2006. Convective transport in nanofluids. *J. Heat Transfer* 128(3): 240-250.

Devi, C.S., Takhar, H.S. & Nath, G. 1991. Unsteady mixed convection flow in stagnation region adjacent to a vertical surface. *Wärme-und Stoffübertragung* 26(2): 71-79.

Ellahi, R., Tariq, M.H., Hassan, M. & Vafai, K. 2017. On boundary layer nano-ferroliquid flow under the influence of low oscillating stretchable rotating disk. *J. Mol. Liq.* 229: 339-345.

Harris, S.D., Ingham, D.B. & Pop, I. 2009. Mixed convection boundary-layer flow near the stagnation point on a vertical surface in a porous medium: Brinkman model with slip. *Transp. Porous Media* 77(2): 267-285.

Hassan, M., Zeeshan, A., Majeed, A. & Ellahi, R. 2017. Particle shape effects on ferrofuids flow and heat transfer under influence of low oscillating magnetic field. *J. Magn. Magn. Mater.* 443: 36-44.

Ibrahim, S.M., Lorenzini, G., Kumar, P.V. & Raju, C.S.K. 2017. Influence of chemical reaction and heat source on dissipative MHD mixed convection flow of a Casson nanofluid over a nonlinear permeable stretching sheet. *Int. J. Heat Mass Transfer* 111: 346-355.

Ingham, D.B. 1986. Singular and non-unique solutions of the boundary-layer equations for the flow due to free convection near a continuously moving vertical plate. *J. Appl. Math. Phys. (ZAMP)* 37(4): 559-572.

Ishak, A., Nazar, R., Bachok, N. & Pop, I. 2010. MHD mixed convection flow adjacent to a vertical plate with prescribed surface temperature. *Int. J. Heat Mass Transfer* 53(21): 4506-4510.

Mabood, F., Ibrahim, S.M., Kumar, P.V. & Khan, W.A. 2017. Viscous dissipation effects on unsteady mixed convective stagnation point flow using Tiwari-Das nanofluid model. *Results Phys*. 7: 280-287.

Mamourian, M., Shirvan, K.M., Ellahi, R. & Rahimi, A.B. 2016. Optimization of mixed convection heat transfer with entropy generation in a wavy surface square lid-driven cavity by means of Taguchi approach. *Int. J. Heat Mass Transfer* 102: 544-554.

Mansur, S., Ishak, A. & Pop, I. 2015. The magnetohydrodynamic stagnation point flow of a nanofluid over a stretching/shrinking sheet with suction. *PLoS One* 10(3): e0117733.

Merkin, J.H. 1986. On dual solutions occurring in mixed convection in a porous medium. *J. Eng. Math*. 20(2): 171-179.

Mohamed, M.K.A., Noar, N.A.Z.M., Salleh, M.Z. & Ishak, A. 2016. Free convection boundary layer flow on a horizontal circular cylinder in a nanofluid with viscous dissipation. *Sains Malaysiana* 45(2): 289-296.

Nazar, R., Noor, A., Jafar, K. & Pop, I. 2014. Stability analysis of three-dimensional flow and heat transfer over a permeable shrinking surface in a Cu-water nanofluid. *International Journal of Mathematical, Computational, Physical, Electrical and Computer Engineering* 8(5): 782-788.

Nazar, R. & Pop, I. 2004. Unsteady mixed convection near the forward stagnation point of a two-dimensional symmetric body prescribed with a constant wall heat flux. *Sains Malaysiana* 33(1): 15-17.

Noor, N.F.M., Haq, R.U., Nadeem, S. & Hashim, I. 2015. Mixed convection stagnation flow of a micropolar nanofluid along a vertically stretching surface with slip effects. *Meccanica* 50(8): 2007-2022.

Othman, N.A., Yacob, N.A., Bachok, N., Ishak, A. & Pop, I. 2017. Mixed convection boundary-layer stagnation point flow past a vertical stretching/shrinking surface in a nanofluid. *Appl. Therm. Eng*. 115: 1412-1417.

Oztop, H.F. & Abu-Nada, E. 2008. Numerical study of natural convection in partially heated rectangular enclosures filled with nanofluids. *Int. J. Heat Fluid Flow* 29(5): 1326-1336.

Rahman, M.M., Merkin, J.H. & Pop, I. 2015. Mixed convection boundary-layer flow past a vertical flat plate with a convective boundary condition. *Acta Mech*. 226(8): 2441-2460.

Ramachandran, N., Chen, T.S. & Armaly, B.F. 1988. Mixed convection in stagnation flows adjacent to vertical surfaces. *J. Heat Transfer* 110(2): 373-377.

Rashidi, S., Akar, S., Bovand, M. & Ellahi, R. 2017. Volume of fluid model to simulate the nanofluid flow and entropy generation in a single slope solar still. *Renew. Energy* 115(C): 400-410.

Ridha, A. & Curie, M. 1996. Aiding flows non-unique similarity solutions of mixed-convection boundary-layer equations. *J. Appl. Math. Phys. (ZAMP)* 47(3): 341-352.

Roşca, A.V., Roşca, N.C. & Pop, I. 2014. Note on dual solutions for the mixed convection boundary layer flow close to the lower stagnation point of a horizontal circular cylinder: Case of constant surface heat flux. *Sains Malaysiana* 43(8): 1239-1247.

Roşca, N.C. & Pop, I. 2017. Axisymmetric rotational stagnation point flow impinging radially a permeable stretching/shrinking surface in a nanofluid using Tiwari and Das model. *Sci. Rep*. 7: 1-11.

Saidur, R., Leong, K.Y. & Mohammad, H.A. 2011. A review on applications and challenges of nanofluids. *Renew. Sust. Energy Rev*. 15(3): 1646-1668.

Shampine, L.F., Kierzenka, J. & Reichelt, M.W. 2000. Solving boundary value problems for ordinary differential equations in MATLAB with bvp4c. *Tutorial Notes* 2000: 1-27.

Shirvan, K.M., Mamourian, M. & Ellahi, R. 2017. Numerical investigation and optimization of mixed convection in ventilated square cavity filled with nanofluid of different inlet and outlet port. *Int. J. Numer. Methods Heat Fluid Flow* 27(9): 2053-2069.

Shirvan, K.M., Mamourian, M., Mirzakhanlari, S. & Ellahi, R. 2017. Numerical investigation of heat exchanger effectiveness in a double pipe heat exchanger filled with nanofluid: A sensitivity analysis by response surface methodology. *Powder Technol*. 313: 99-111.

Subhashini, S.V., Sumathi, R. & Momoniat, E. 2014. Dual solutions of a mixed convection flow near the stagnation point region over an exponentially stretching/shrinking sheet in nanofluids. *Meccanica* 49(10): 2467-2478.

Tiwari, R.K. & Das, M.K. 2007. Heat transfer augmentation in a two-sided lid-driven differentially heated square cavity utilizing nanofluids. *Int. J. Heat Mass Transfer* 50(9): 2002-2018.

Weidman, P.D., Kubitschek, D.G. & Davis, A.M.J. 2006. The effect of transpiration on self-similar boundary layer flow over moving surfaces. *Int. J. Eng. Sci*. 44(11): 730-737.

Zaimi, K., Ishak, A. & Pop, I. 2017. Unsteady flow of a nanofluid past a permeable shrinking cylinder using Buongiorno's model. *Sains Malaysiana* 46(9): 1667-1674.

Zeeshan, A., Hassan, M., Ellahi, R. & Nawaz, M. 2017a. Shape effect of nanosize particles in unsteady mixed convection flow of nanofluid over disk with entropy generation. *P.I. Mech. Eng. E-J. Pro*. 231(4): 871-879.

Zeeshan, A., Shehzad, N. & Ellahi, R. 2017b. Analysis of activation energy in Couette-Poiseuille flow of nanofluid in the presence of chemical reaction and convective boundary conditions. *Results Phys*. 8: 502-512.

Anuar Jamaludin
Department of Mathematics
Universiti Pertahanan Nasional Malaysia
57000 Kuala Lumpur, Federal Territory
Malaysia

Roslinda Nazar*
School of Mathematical Sciences
Faculty of Science and Technology
Universiti Kebangsaan Malaysia
43600 UKM Bangi, Selangor Darul Ehsan
Malaysia

Ioan Pop
Department of Mathematics
Babeş-Bolyai University
R-400084 Cluj-Napoca
Romania

*Corresponding author; email: rmn@ukm.edu.my

Received: 31 March 2018
Accepted: 22 May 2018